

Deviations from generalized equipartition in confined, laser-cooled atoms

Gadi Afek,^{*} Alexander Cheplov[✉], Arnaud Courvoisier, and Nir Davidson

Department of Physics of Complex Systems, Weizmann Institute of Science, Rehovot 76100, Israel

 (Received 5 October 2019; accepted 9 March 2020; published 23 April 2020)

We observe a significant steady-state deviation from the generalized equipartition theorem, one of the pivotal results of classical statistical mechanics, in a system of confined, laser-cooled atoms. We parametrize this deviation, measure its dynamics, and show that its steady-state value quantifies the departure of nonthermal states from thermal equilibrium even for anharmonic confinement. In particular, we find that deviations from equipartition grow as the system dynamics becomes more anomalous. We present numerical simulations that validate the experimental data and reveal an inhomogeneous distribution of the kinetic energy through the system, supported by an analytical examination of the phase space.

DOI: [10.1103/PhysRevA.101.042123](https://doi.org/10.1103/PhysRevA.101.042123)

I. INTRODUCTION

The 100-year-old generalized equipartition theorem [1], one of the cornerstones of classical statistical physics, remains of great interest throughout various fields of research to this day [2–4]. It states that for a system at thermal equilibrium with a heat bath of temperature T , for any generalized coordinate q_i and Hamiltonian \mathcal{H} ,

$$\left\langle q_i \frac{\partial \mathcal{H}}{\partial q_j} \right\rangle = \delta_{ij} k_B T, \quad (1)$$

where k_B is the Boltzmann constant, δ_{ij} is the Kronecker delta, and $\langle \dots \rangle$ denotes ensemble averaging. An immediate result of this theorem is the well-known equipartition theorem [5,6], valid for degrees of freedom which appear quadratically in the Hamiltonian, in which case the relations implies an equal distribution of energy among these degrees of freedom. Other significant extensions have been shown for finite-sized systems [7], generalized canonical ensembles [8], and nonextensive thermodynamics [9]. While the equipartition theorem is strictly correct only at thermal equilibrium, it was extended and applied to other thermodynamic systems and observed to hold even outside of thermal equilibrium [10].

Ultracold atomic systems have been furthering the understanding of statistical physics for several decades and have recently begun to be used to explore aspects of nonequilibrium physics [11–15]. An especially interesting system for probing nonequilibrium statistical mechanics is that of ultracold atomic ensembles in dissipative one-dimensional (1D) optical lattices, where the heat bath is implemented by the electric field of the lattice lasers. The main advantage of such a system is the unique control over experimental parameters, allowing fine-tuning of the dynamics. In addition to its being an experimentally and theoretically well-established test bed for anomalous dynamics [16–33], it has recently been linked

with the notion of nonthermal equilibrium [34,35]. Through extensive analysis of the phase-space dynamics of such a system confined in a harmonic potential, a prediction has been put forth of a violation, under certain conditions, of the equipartition theorem.

In this paper, we present a detailed experimental investigation of the steady-state deviation from equipartition for trapped, laser-cooled atoms in contact with a nonthermal heat bath, implemented by a 1D, dissipative optical lattice. For completion, we also investigate numerically the effect of anharmonicity of the confining potential on the dynamics and magnitude of this deviation. Finally, as a basis for further work, we present a prediction of the position dependence of the local kinetic energy for such confined Sisyphus cooled atoms, supported by analytics and numerics.

II. EXPERIMENTAL PROCEDURE

A. Using the equipartition theorem to quantify departure from thermal equilibrium

Any departure from thermal equilibrium of a 1D confined system with coordinates (x, p) and Hamiltonian \mathcal{H} can be parametrized using the *equipartition parameter* χ [34,35],

$$\chi \equiv \sqrt{\left\langle p \frac{\partial \mathcal{H}}{\partial p} \right\rangle \left\langle x \frac{\partial \mathcal{H}}{\partial x} \right\rangle}, \quad (2)$$

which depends explicitly on the details of the confining potential. Given that $\chi = 1$ for systems at thermal equilibrium, deviations of χ from unity imply nonthermal distributions and a possible break of energy-probability equivalence. For the simple case of harmonic confinement, one can derive the harmonic equipartition parameter χ_H from Eq. (2),

$$\chi_H \equiv \frac{\sigma_v}{\omega \sigma_x}, \quad (3)$$

where σ_x and σ_v are the respective standard deviations of the position and velocity distributions (both of which are Gaussian for a harmonic potential and thermal equilibrium), and ω is the harmonic trap frequency. χ_H is a leading-order

^{*}Present address: Wright Laboratory, Department of Physics, Yale University, New Haven, Connecticut 06520, USA; gadi.afek@yale.edu

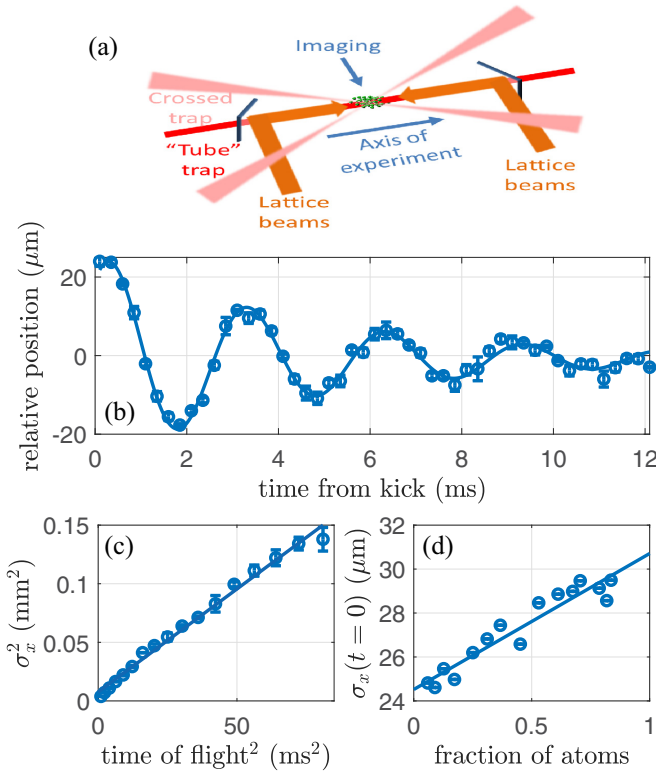


FIG. 1. Measurement scheme for the equipartition parameter, $\chi_H \equiv \sigma_v/\omega\sigma_x$. (a) Sketch of the experimental setup. Laser-cooled ^{87}Rb atoms are trapped in a crossed dipole trap (light red) overlapped with a strong, single-beam tube trap (dark red) and coupled to a nonthermal heat bath implemented by with a set of 1D Sisyphus cooling lattice beams (orange) through dichroic mirrors. The atoms propagate in this combined potential and are subsequently imaged. (b) The trapped cloud is kicked with a short, directional pulse of near-resonant light to excite subsequent center-of-mass oscillations, and the center-of-mass position is extracted (circles). The trap frequency ω is calculated by fitting the data to an exponentially decaying sine. The decay of the center-of-mass oscillations is attributed to anharmonicity of the confining potential. (c) Typical result of a time-of-flight experiment (circles), with a fit to $\sigma_x^2(\tau) = \sigma_x^2(\tau=0) + \sigma_v^2\tau^2$ (solid line). (d) Size of the atomic cloud, obtained by scanning the number of atoms, and hence the density, in the trap and extrapolating to zero density using microwave pulses (blue circles; see text). The solid line is a linear fit. The data presented in (b)–(d) corresponds to measurements at thermal equilibrium, yielding the value of $\chi_H = 0.82 \pm 0.02$.

approximation of χ for any continuous potential with a minimum and is, in practice, considerably easier to access experimentally than χ for many systems.

B. Experiment

In the experiment [Fig. 1(a)], a cloud of ^{87}Rb atoms is magneto-optically trapped and then cooled down to a temperature of ~ 20 μK . The final cooling step is optical evaporation in a far-detuned, 1064-nm crossed dipole trap focused down to a waist of 60 μm overlapped with a strong, $\sim 180\text{-W}$, single-1070-nm-beam tube trap (YLR-200-LP-AC-Y14; IPG photonics), loosely focused to a waist of 120 μm to provide

strong confinement in the radial direction while leaving the axial dynamics practically unaffected. The Rayleigh length of the beam is >4 cm, much larger than any other relevant length scale. Extra care is taken to avoid reflections that may cause interference affecting the dynamics. The $>2\text{-s}$ -long evaporation, much longer than the $\sim 100\text{-ms}$ collision time, leaves the atoms at thermal equilibrium with the confining potential [36]. The atoms are then coupled for a duration t to a nonthermal heat bath, implemented using a 1D dissipative Sisyphus lattice, where they may exhibit anomalous dynamics, depending on the modulation depth of the lattice U_0 [25,33]. Set by the power and detuning of the lattice beams from the relevant atomic transition, U_0 is the main control parameter of the experiment. The other experimental parameters are similar to those in [33]. The trap depth is ~ 3 MHz, small compared to the $\sim 60\text{-MHz}$ detuning of the lattice, rendering trap-induced differential ac Stark shifts negligible. Each measurement of the equipartition parameter $\chi_H(U_0, t)$ is comprised of three separate experiments: trap oscillations, time of flight, and extrapolation to zero density of an *in situ* image of the cloud, giving access to the information needed to calculate the equipartition parameter of Eq. (3). The *in situ* absorption images are taken as the cloud is released from the trap, capturing both the atoms trapped in the focus and those held in the area of the beams removed from the overlapped foci. To ensure that we do not wrongly include these atoms in our analysis, we fit the data to a sum of two Gaussians and use the narrower one [37].

Figure 1(b) shows a typical trap oscillation experiment, in which center-of-mass oscillations are excited using a short, near-resonant light pulse. The atoms are sequentially imaged as a function of the time elapsed after the pulse. The measured frequency is $\omega = 2\pi \times (332 \pm 2)$ Hz (used throughout the paper), with approximately 1.6 oscillations before $1/e$ decay of the contrast, attributed to dephasing of the ensemble-averaged oscillations due to the anharmonicity of the confining potential. The trap frequency itself is unaffected by anharmonicity for atoms much colder than the trap depth.

The width of the velocity distribution is measured using time of flight. The cloud is released and allowed to expand in one dimension for a time τ within the tube trap. Its size is fitted with the relation $\sigma_x^2(\tau) = \sigma_x^2(\tau=0) + \sigma_v^2\tau^2$ between the standard deviation of the spatial distribution $\sigma_x(\tau)$ and that of the velocity distribution σ_v . Figure 1(c) shows the result of such a measurement, giving $\sigma_v = 42 \pm 1$ mm/s. We verify that scattered light from the unidirectional tube trap does not affect the dynamics substantially by allowing the atoms to expand in it for a relatively long time (>100 ms; much longer than the duration of the experiment) and verifying that the center of mass of the cloud does not shift due to scattering of trap photons by more than 1% compared to its initial position.

Measuring the *in situ* cloud size is challenging, mostly due to the optical density of the clouds, biasing the output of our absorption imaging. To alleviate this, we excite a controlled, variable fraction of the atoms homogeneously into the $F = 2$ hyperfine state using a microwave pulse, scanning the density of the atoms in a given trap while leaving the density profile unchanged [38]. The transferred atoms are imaged using state-selective absorption imaging and the cloud size is extracted from fitting the distribution. The obtained

values are then fitted with a linear relation and extrapolated down to zero atoms, representing zero density, as the trap does not change. This gives the unbiased cloud size. Figure 1(d) shows a result of such a measurement, yielding $\sigma_x(t=0) = 24.5 \pm 0.3 \mu\text{m}$. Combining these we get, for atoms at thermal equilibrium after a long period of evaporative cooling, $\chi_H = 0.82 \pm 0.02$, where the error is of statistical origin. Considering the possible systematics in such a measurement, one needs to look at the factors affecting each of the three measurements. Time of flight is a well-established technique, increasing in precision as the cloud is allowed to expand more and more compared to its initial size. Our “tube” trap allows these long measurement times, as it prevents the atoms from expanding in the radial direction. We have also compared the time-of-flight results to a spectroscopic Raman velocity selective measurement, obtaining agreement to within 5%–10%. Trap oscillations are measured very precisely and with small error bars. This can also be verified independently by looking at revival periods of quantum coherence imprinted with Raman control and is in very good agreement [39]. The initial cloud size is a challenging measurement due to systematics arising from high densities in the trap and limited imaging resolution. To further verify this we performed yet another measurement, scanning the density in a different way. Instead of using a microwave pulse to homogeneously transfer atoms to the excited state and imaging them, we scan the initial magneto-optical trap (MOT) power and effectively begin the experiment with a variable number of atoms in the same-sized dipole trap. The results agree well, to within less than 5%. The fact that anharmonicity in a typical optical trap is much more substantial than simple Gaussian corrections has been previously established and verified with spectroscopic tools, much more accurate and susceptible to different types of systematics [39]. We can therefore conservatively bound the systematic error on our measurement of χ_H from above at the 10% limit. The deviation of this result from the theoretical unity value is related to the anharmonicity of the confining potential and is elaborated on later.

III. RESULTS AND DISCUSSION

A. Dynamics and steady state

Figure 2 describes the dynamics of the equipartition parameter of the ensemble χ_H under coupling to both the confining potential and the nonthermal heat bath, compared to the case of thermal equilibrium with the optical trap. Figure 2(a) shows the number of atoms remaining in the trap as a function of the lattice exposure time and depth. For deep lattices losses are substantial (up to a factor of about 10), mostly due to radial heating from photon scattering in the directions orthogonal to the lattice beams [25].

The dynamics of the equipartition parameter is given in Fig. 2(b), taking into account the trap oscillation frequency measured in Fig. 1(b) and calculating $\chi_H(U_0, t)$ according to Eq. (3). Each symbol represents set of the three experiments described above, sampled 20 times in random order. Error bars are evaluated by considering the 67% confidence intervals of the linear fits used to determine $\sigma_x(t=0)$ and σ_v . Solid lines are fits performed by taking the short-time data, $t < 1.2$ ms, and fitting it to $A \exp(-\gamma t) + C$ to get the decay rate γ . Then

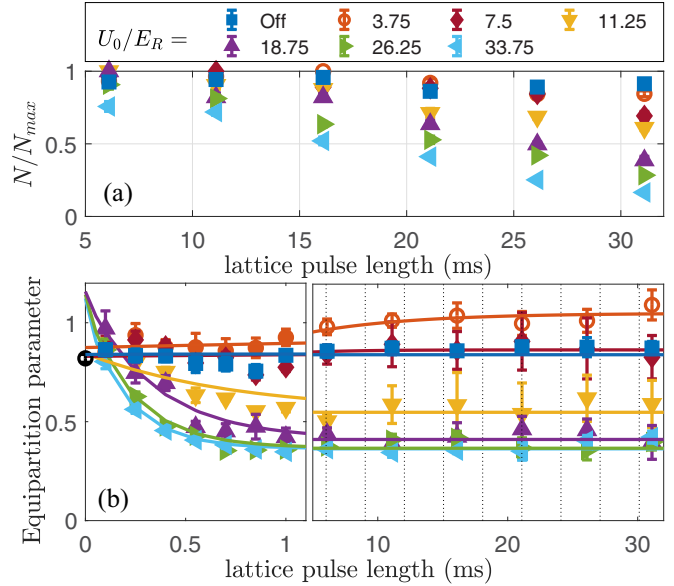


FIG. 2. Dynamics of the equipartition parameter χ_H . (a) Number of remaining atoms in the trap as a function of the exposure time and lattice depth of the Sisyphus lattice. (b) Equipartition parameter per Sisyphus lattice depth and exposure time. Left panel, short times; right panel, long times. Blue squares correspond to thermal dynamics; other colored symbols, to anomalous dynamics. The black circle at $t=0$ represents the value obtained in Figs. 1(b)–1(d), according to Eq. (3). Solid lines are exponential fits (see text). Dotted vertical lines are integer multiples of the trap oscillation period.

all the data is included and fitted to $(\chi_0 - \chi_\infty) \exp(-\gamma t) + \chi_\infty$, with the γ from the short-time fit. The fact that this is indeed a steady-state value and not a transient effect is proven by waiting many trap oscillation periods, shown by dashed vertical lines in Fig. 2(b), right panel. Density-dependent effects such as s -wave atomic collisions and light-assisted repulsion [40] can be ruled out since despite the fact that the number of remaining atoms in the trap, and hence the density of the confined atoms, changes by up to an order of magnitude, smooth behavior of the equipartition parameter is observed. The fast time scale of the dynamics of χ_H is determined primarily by that of the velocity dynamics. Our simulations indicate that the slower time scale is related to that of the relaxation of the position distribution. Note that for shallow lattices the dynamics becomes extremely slow [24,41], hence for the $U_0/E_R = 3.75$ data set (red circles) there is no obvious steady state achieved within the duration of the experiment. We use E_R , the recoil energy for the ^{87}Rb D_2 line, as the relevant energy scale. Figure 3 shows the RMS position and velocity [Figs. 3(a) and 3(b), respectively] for the data shown in Fig. 2. Except for the deepest lattices, the relevant time scale for reaching the nonequilibrium steady state is that of the trap oscillation period. We are able to evolve the system for ~ 10 oscillation periods, allowing all thermodynamic variables to reach steady state. This is even further verified in Figs. 3(c)–3(e), which show an additional ~ 5 oscillation periods for midrange lattice depths.

We summarize the steady-state values of the harmonic equipartition parameter as a function of the lattice depth in

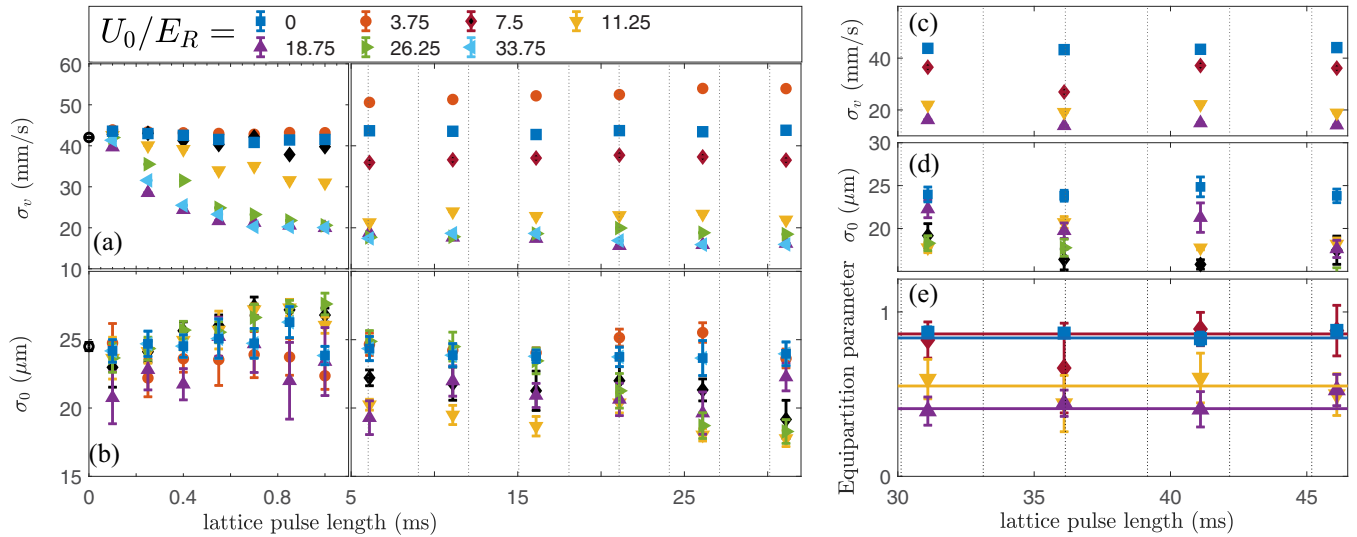


FIG. 3. (a) RMS position and (b) velocity as a function of the exposure time and lattice depth of the Sisyphus lattice for the data shown in Fig. 2. Long-time measurements of (c) the position, (d) the velocity, and (e) χ_H taken for a select number of lattice depths, where atom loss was not a limiting factor in the measurement.

Fig. 4. The thermal value corresponds to the lattice being turned off. As the lattice gets deeper, the steady-state value is reduced, in accordance with the theoretical prediction [34,35]. The value of the equipartition parameter was predicted to begin to climb back towards its thermal value with a further increase in the depth of the lattice, however, we were not able to observe this behavior due to experimental constraints. The steady-state χ_H values for shallow lattices are higher than the equilibrium value. We attribute these deviations to residual heating of the atoms in shallow lattices [16,18,22,25], consistent with Eq. (3).

B. Effects of anharmonicity of the confining potential

We now return to the interpretation of the deviation from unity of the measured thermal value of $\chi_H = 0.82 \pm 0.02$ (Figs. 1 and 2). Deviations of χ_H from unity are caused by two independent factors. The first is the anharmonicity of the

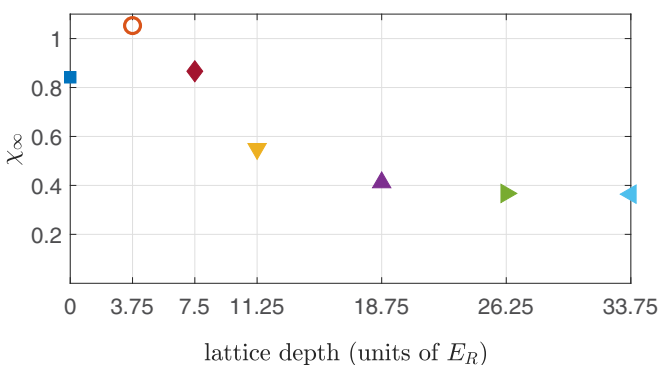


FIG. 4. Steady-state equipartition parameter as a function of the lattice depth [extracted from the exponential fit in Fig. 2(b)]. Error bars are smaller than the symbol size. High Sisyphus lattice powers significantly decrease the values of χ_H from their thermal value.

confining potential. It has recently been shown [39] that the anharmonicity of the confining potential plays a pivotal role in determining the dynamical properties of the system. To see how it affects the equipartition parameter, we perform a measurement of χ_H as a function of the temperature, obtained by varying the depth of the final optical evaporative cooling stage. We do so for both axes of the trap, horizontal (in which the main experiment is performed) and vertical. The horizontal axis suffers from greater anharmonicity due to residual trapping of atoms outside of the crossed region of the dipole trap (“wings”). This is manifested in a substantial decay that occurs after a smaller number of trap oscillations compared to that of the vertical axis. The effect, depicted in Fig. 5, is twofold: As the temperature is lowered, the ratio between the energy of the atoms and the depth of the trap is reduced and the atoms sample less anharmonicity, bringing about an approach to unity of the equipartition parameter for both axes. The vertical axis gives a higher equipartition parameter throughout the temperature range, attributed to the fact that the anharmonicity there is inherently lower. In the experiment we measure χ_H , rather than χ_G , a Gaussian equipartition parameter that can be obtained directly from Eq. (1), due to experimental considerations. Assuming a purely Gaussian type of anharmonicity, described by the Hamiltonian $\mathcal{H} = p^2/(2m) - A \exp[-x^2/(2\sigma_T^2)]$, where A is the depth of the potential and σ_T its width, and defining $\alpha \equiv \sigma_x/\sigma_T$, the size of the atomic distribution relative to the size of the trap, and $\beta \equiv k_B T/A = \alpha/(1 + \alpha)^{3/2}$, the temperature of the atoms relative to the depth of the trap, one can derive analytically a scaling relation between χ_H and the temperature, $\chi_H = \sqrt{\beta/\alpha}$ [37]. We use this relation to fit the data in Fig. 5, with good agreement up to a separate initial value for $\chi_H(T = 0)$ used as a fit parameter to account for different inherent anharmonicity between the axes.

Figure 6 presents numerical simulations comparing values of χ_H for normal diffusion, i.e., thermal equilibrium and no

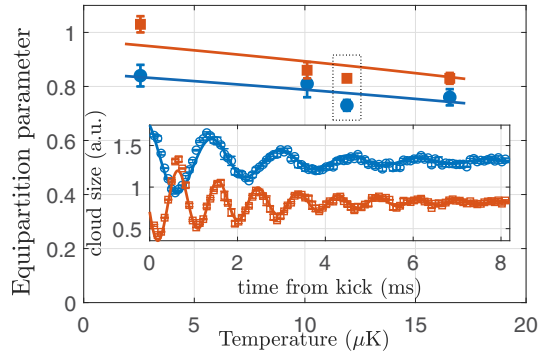


FIG. 5. (a) χ_H as a function of the temperature, scanned by varying the depth of the final optical evaporative cooling stage, of a 3D trapped ensemble for two axes: horizontal (blue circles) and vertical (red squares). Inset: A measurement of the trapping oscillations, taken for the χ_H values in the dotted rectangle. More oscillations prior to substantial decay are observed on the vertical axis, indicating higher harmonicity. Solid lines are best fits to the proportionality relation for χ_H in a Gaussian trap described in the text.

Sisyphus lattice, for harmonic (blue triangles) and anharmonic Gaussian (gold squares) traps. The horizontal axis is the dimensionless diffusion constant, which for normal diffusion is proportional to the temperature of the atoms. For a harmonic trap $\chi_H = 1$ for all temperatures. For the anharmonic trap, as the temperature increases the atoms sample more anharmonicity and the harmonic equipartition parameter diminishes. This is the effect we associate with our thermal equilibrium result. The reason the effect in the experiment is more pronounced

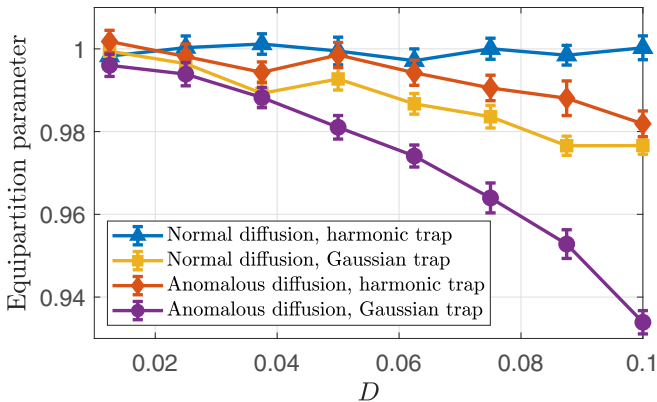


FIG. 6. Monte Carlo simulation of steady-state χ_H for harmonic and Gaussian anharmonic trapping potentials, as a function of the dimensionless diffusion coefficient D . For normal diffusion (thermal equilibrium, no Sisyphus lattice, $D \sim T$, the temperature of the atoms) in a harmonic trap (blue triangles), equipartition holds for all values of the diffusion coefficient. In an anharmonic trap, the hotter the atoms are, the more anharmonicity they experience, increasing the deviation from unity. Anomalous diffusion (nonthermal equilibrium, Sisyphus lattice on, $D \sim E_R/U_0$, the inverse lattice depth) generates deviations from unity even for harmonic potentials (red diamonds). The effect of anomalous dynamics combined with the anharmonic potential is additive in the decrease in χ_H (purple circles).

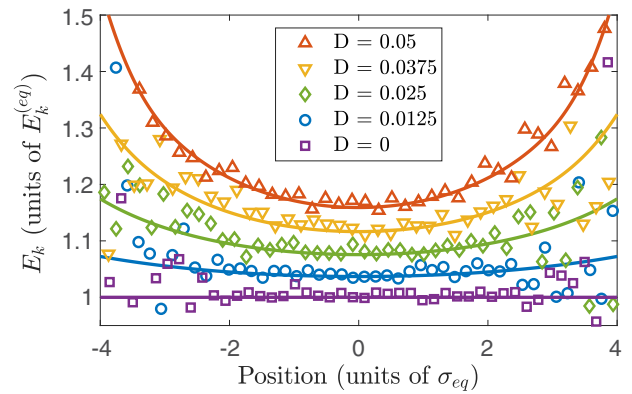


FIG. 7. Dependence of the kinetic energy, normalized by its equilibrium value, on position, normalized by the equilibrium Gaussian RMS value, at the steady state of anomalous dynamics in a harmonic trap, calculated independently numerically (markers) and analytically (solid lines). The case of $D = 0$ represents thermal equilibrium normal diffusion. For higher D values the local kinetic energy shows a stronger dependence on position [37].

is that Gaussian anharmonicity does not suffice to describe the real anharmonicity typical for dipole traps [39]. It is still, however, very useful for simplification of calculations and qualitative analysis. The second factor contributing to the decay is the main result of this paper. The predicted behavior of the harmonic potential [34,35] is reobtained in our simulations, using the reduced semiclassical Sisyphus cooling mechanism in the regime of deep lattices, where the dimensionless diffusion coefficient is $\sim E_R/U_0$ (Fig. 6; red diamonds). Finally, we show (purple circles) that the two effects are additive, confirming our experimental results and showing that the breakdown of equipartition persists in anharmonic potentials and χ_H is a fair predictor of it [42]. Our simulations further indicate a violation of equipartition for yet another interesting class of anharmonic perturbations: logarithmically corrected harmonic potentials [37]. Agreement between the experiment and the theoretical predictions is qualitative. This is not new for this system [25,33] and is mostly attributed to the complex atomic level structure ignored by the semiclassical model of Sisyphus cooling.

C. Inhomogeneous distributions of the kinetic energy

The steady-state phase-space representation of the system has been theoretically studied in [35]. It was found that equivalence between equienergetic and equiprobable surfaces no longer holds. Another fascinating aspect can be revealed by studying correlations of the kinetic energy, $\sim v^2$, with the position. Specifically, the kinetic energy is found to be inhomogeneous, i.e., position dependent. In Fig. 7 we present the results of our analytics and numerics, using the methods described in [35]. The local average kinetic energy was calculated as the marginal expectation value of the kinetic energy term with respect to the total phase-space probability distribution function at a fixed position. The two methods are in good agreement. Note that different units are used in Figs. 6 and 7, resulting in a slightly different interpretation of D [37]. The results imply inseparability of the phase-space probability

distribution function, in contrast to thermal distributions, and enhanced kinetic-potential energy correlations. The inhomogeneity of the kinetic energy at steady state can serve as direct evidence of the nonthermal nature of the Sisyphus dissipative lattice.

In recent work [33], we put forth a technique enabling direct imaging of the phase-space density distribution function of an atomic ensemble. Utilizing a higher-order version of this method, studying correlations of the kinetic energy, $\sim v^2$, with the position, it may be possible to observe this position dependence of the kinetic energy, testing our prediction.

IV. SUMMARY AND OUTLOOK

In summary, we present a detailed experimental observation of the previously overlooked deviation from generalized equipartition in dilute, confined, laser-cooled atoms, looking

not only at the steady-state behavior but also at the dynamics. We introduce the equipartition parameter, which can serve to quantify the departure from thermal equilibrium of non-thermal states and establish its relation to the anharmonicity of the confining potential. With improved signal to noise it should be interesting to attempt a direct measurement of χ [Eq. (2)] involving the full details of the confining potential. Finally, we present a prediction of inhomogeneous kinetic and potential energies for the system of confined, laser-cooled atoms, supported by analytical and numerical methods and experimentally attainable.

ACKNOWLEDGMENTS

The authors would like to thank Eli Barkai, Andreas Dechant, David Mukamel, and Oren Raz for fruitful discussions.

-
- [1] R. C. Tolman, *Phys. Rev.* **11**, 261 (1918).
- [2] M. J. Uline, D. W. Siderius, and D. S. Corti, *J. Chem. Phys.* **128**, 124301 (2008).
- [3] C. Maggi, M. Paoluzzi, N. Pellicciotta, A. Lepore, L. Angelani, and R. Di Leonardo, *Phys. Rev. Lett.* **113**, 238303 (2014).
- [4] K. Chen, D. He, and H. Zhao, *Sci. Rep.* **7**, 3460 (2017).
- [5] J. J. Waterston and L. Rayleigh, *Philos. Trans. R. Soc. London A* **183**, 1 (1892).
- [6] L. Boltzmann, *Ann. Phys.* **236**, 175 (1877).
- [7] P. A. Mello and R. F. Rodríguez, *Am. J. Phys.* **78**, 820 (2010).
- [8] H. L. Frisch, *Phys. Rev.* **91**, 791 (1953).
- [9] S. Martinez, F. Pennini, A. Plastino, and C. Tessone, *Physica A: Stat. Mech. Appl.* **305**, 48 (2002).
- [10] K. Nichol and K. E. Daniels, *Phys. Rev. Lett.* **108**, 018001 (2012).
- [11] S. Diehl, A. Micheli, A. Kantian, B. Kraus, H. P. Büchler, and P. Zoller, *Nat. Phys.* **4**, 878 (2008).
- [12] S. Diehl, E. Rico, M. A. Baranov, and P. Zoller, *Nat. Phys.* **7**, 971 (2011).
- [13] D. S. Lobser, A. E. S. Barentine, E. A. Cornell, and H. J. Lewandowski, *Nat. Phys.* **11**, 1009 (2015).
- [14] F. Kindermann, A. Dechant, M. Hohmann, T. Lausch, D. Mayer, F. Schmidt, E. Lutz, and A. Widera, *Nat. Phys.* **13**, 137 (2016).
- [15] D. Mayer, F. Schmidt, S. Haupt, Q. Bouton, D. Adam, T. Lausch, E. Lutz, and A. Widera, [arXiv:1901.06188](https://arxiv.org/abs/1901.06188).
- [16] Y. Castin, J. Dalibard, and C. Cohen-Tannoudji, in *Light Induced Kinetic Effects on Atoms, Ions, and Molecules*, edited by L. Moi *et al.* (ETS Editrice, Pisa, 1991), p. 5.
- [17] S. Marksteiner, K. Ellinger, and P. Zoller, *Phys. Rev. A* **53**, 3409 (1996).
- [18] H. Katori, S. Schlipf, and H. Walther, *Phys. Rev. Lett.* **79**, 2221 (1997).
- [19] E. Lutz, *Phys. Rev. A* **67**, 051402(R) (2003).
- [20] E. Lutz, *Phys. Rev. Lett.* **93**, 190602 (2004).
- [21] J. Jersblad, H. Ellmann, K. Stöckel, A. Kastberg, L. Sanchez-Palencia, and R. Kaiser, *Phys. Rev. A* **69**, 013410 (2004).
- [22] P. Douglas, S. Bergamini, and F. Renzoni, *Phys. Rev. Lett.* **96**, 110601 (2006).
- [23] D. A. Kessler and E. Barkai, *Phys. Rev. Lett.* **105**, 120602 (2010).
- [24] O. Hirschberg, D. Mukamel, and G. M. Schütz, *Phys. Rev. E* **84**, 041111 (2011).
- [25] Y. Sagi, M. Brook, I. Almog, and N. Davidson, *Phys. Rev. Lett.* **108**, 093002 (2012).
- [26] D. A. Kessler and E. Barkai, *Phys. Rev. Lett.* **108**, 230602 (2012).
- [27] A. Dechant and E. Lutz, *Phys. Rev. Lett.* **108**, 230601 (2012).
- [28] A. Wickenbrock, P. C. Holz, N. A. A. Wahab, P. Phoonthong, D. Cubero, and F. Renzoni, *Phys. Rev. Lett.* **108**, 020603 (2012).
- [29] E. Barkai, E. Aghion, and D. A. Kessler, *Phys. Rev. X* **4**, 021036 (2014).
- [30] A. Dechant, E. Lutz, D. A. Kessler, and E. Barkai, *Phys. Rev. X* **4**, 011022 (2014).
- [31] V. Zaburdaev, S. Denisov, and J. Klafter, *Rev. Mod. Phys.* **87**, 483 (2015).
- [32] P. C. Holz, A. Dechant, and E. Lutz, *Europhys. Lett.* **109**, 23001 (2015).
- [33] G. Afek, J. Coslovsky, A. Courvoisier, O. Livneh, and N. Davidson, *Phys. Rev. Lett.* **119**, 060602 (2017).
- [34] A. Dechant, D. A. Kessler, and E. Barkai, *Phys. Rev. Lett.* **115**, 173006 (2015).
- [35] A. Dechant, S. T. Shafier, D. A. Kessler, and E. Barkai, *Phys. Rev. E* **94**, 022151 (2016).
- [36] W. Ketterle and N. V. Druten, in *Advances In Atomic, Molecular, and Optical Physics* (Elsevier, Amsterdam, 1996), pp. 181–236.
- [37] See Supplemental Material at <http://link.aps.org/supplemental/10.1103/PhysRevA.101.042123> for details of the fitting procedures, numerical methods, and more simulation results.
- [38] S. Tung, G. Lamporesi, D. Lobser, L. Xia, and E. A. Cornell, *Phys. Rev. Lett.* **105**, 230408 (2010).
- [39] G. Afek, J. Coslovsky, A. Mil, and N. Davidson, *Phys. Rev. A* **96**, 043831 (2017).

- [40] T. Walker, D. Sesko, and C. Wieman, *Phys. Rev. Lett.* **64**, 408 (1990).
- [41] O. Hirschberg, D. Mukamel, and G. M. Schütz, *J. Stat. Mech.: Theory Exp.* (2012) P02001.
- [42] Within the semiclassical model [16,17], one can come up with a unit transformation under which $D \sim E_R/U_0$, the dimensionless

diffusion constant, is proportional to the inverse depth of the lattice (full derivation and interpretation of other parameters given in [37]). For normal diffusion, under the same unit transformation D is the usual momentum diffusion coefficient given by the Einstein relation $D_p = \gamma m k_B T$, proportional to the temperature of the bath .